Torsional effect on track support structures of railway turnouts crossing impact

Sae Siew, James ; Mirza, Olivia ; Kaewunruen, Sakdirat

DOI:
10.1061/JTEPBS.0000004

Document Version
Peer reviewed version

Citation for published version (Harvard):
Sae Siew, J, Mirza, O & Kaewunruen, S 2017, 'Torsional effect on track support structures of railway turnouts crossing impact', *Journal of Transportation Engineering, Part A: Systems*, vol. 143, no. 2. https://doi.org/10.1061/JTEPBS.0000004

REVISION OF TECHNICAL PAPER

"Torsional effect on track support structures of railway turnouts crossing impact"

(Title contains 11 words)

by

James Sae Siew
School of Civil Engineering
University of Western Sydney, Penrith, NSW, Australia

Olivia Mirza
School of Civil Engineering
University of Western Sydney, Penrith, NSW, Australia

and

Sakdirat Kaewunruen
Birmingham Centre for Railway Research and Education,
University of Birmingham, Birmingham, UK

Submitted to
ASCE Journal of Transportation Engineering

Corresponding Author:

Sakdirat Kaewunruen
Senior Lecturer in Railway and Civil Engineering
School of Engineering, University of Birmingham, Birmingham, UK
e-mail: s.kaewunruen@bham.ac.uk

Manuscript Summary:

Total pages	29	(including 1-page cover)
Number of figures	13	
Number of tables	2	

Torsional effect on track support structures of railway turnouts crossing impact

James Sae Siew[1], Olivia Mirza[2], and Sakdirat Kaewunruen[3]

Abstract: The introduction of special crossings and rail turnouts provides flexibility in the rail network as it allows for vehicles to switch between various tracks, therefore maximizing the utilisation of current infrastructure. Turnouts are a costly and critical feature to a rail system as they suffer adverse operational loads, in comparison to a straight rail track, and thus require regular maintenance. This leads to the question of whether a turnout can be justified for flexibility in comparison to upkeep costs throughout the life of the turnout. Therefore, great consideration is given to the interaction between the turnout components, and reducing wear in service, as failed components may have adverse effects on the performance of neighbouring components. This paper herein presents a development of 3D finite element (FE) model, fostering nonlinearities in materials' behaviours, in order to analyse the forces and reactions within a railway turnout system. The analysis provide new findings of critical sections within the turnout and further enables alterations to be made to initial design of members in order to accommodate for the increased effects. The FE model comprises of standard concrete sleepers with 60 kg/m rail, and with a tangential turnout radius of 250 m. The turnout structure is supported by a ballast layer, which is represented by a deformable solid. The FE model is the world first to predict the torsional behaviour of the turnout and its fragile support by considering multi-wheel impacts which would simulate in-service and cyclic loading, and will be adapted as a set of concentrated loads to represent a coupled locomotive negotiating the turnout. The simulations demonstrate the significance of the third medium to suppress the torsional effect of the crossing forces on supporting bearers.

Keywords: Torsional effect; Turnouts; Railroad; Dynamic analysis; Ballasted railway track; Bearers, Sleepers; Crossties.

[1] Formerly Honours Student in Civil Engineering Program, School of Civil Engineering, University of Western Sydney, Penrith, NSW 2057 Australia

[2] Senior Lecturer in Civil Engineering, School of Civil Engineering, Western Sydney University, Penrith, NSW 2057 Australia; e-mail: o.mirza@westernsydney.edu.au

[3] Corresponding author; Birmingham Centre for Railway Research and Education, School of Engineering, University of Birmingham, Birmingham, UK. e-mail: s.kaewunruen@bham.ac.uk; sakdirat@hotmail.com, Formerly, Technical Specialist, RailCorp, Sydney NSW 2000 Australia; and a visiting executive fellow at Department of Civil and

Introduction

One of the great accomplishments during the early 19th century was the development of railways. The realisation of railways spurred exponential industrial growth for it enabled this mode of land transportation, which focuses on mass-freightage, to be reliable and economical. The effectiveness of rail is based upon the general concept of providing a track that is both minimal in space and material, and yet be able to provide a low-friction, guided medium. The introduction of special crossings and turnouts provided flexibility in the rail network as it allowed for vehicles to switch between various tracks, and in-turn reducing the amount of tracks needed.

A turnout is a critical part of the railway where a track crosses over one another at an angle to divert a train from the original track. The railway track and turnouts consists of rails, switches, crossings, sleeper plates, sleepers, ballast and subgrade (as shown in Figure 1). As above mentioned, turnouts are an essential part of a rail system as they provide great flexibility, but at the same time, turnouts are a costly feature to a rail system as they suffer adverse operational loads, in comparison to an open plain rail track, and require regular maintenance. This leads to the question of whether a turnout can be justified for flexibility in comparison to the cost of maintenance throughout the life of the turnout. Turnout components can be designed with stronger, hard wearing materials as an option to help reduce maintenance costs. When designing, and maintaining, the railway systems, great consideration is given to the interaction between the turnout components in service. Due to the particular geometry of wheel–rail contact and sudden variation of track flexibility, severe impact loads may occur during train passage over the turnout. Turnout components are subjected to general wear, rolling contact fatigue and accumulated irreversible (plastic) deformations (Kassa and Nielsen, 2008a; Kaewunruen, 2010, 2013a; 2013b).

During their life cycles, railway track structures experience static, dynamic and often impact loading conditions due to wheel/rail interactions associated with the abnormalities in either a wheel or a rail. Especially at turnouts crossing, the wheel rail interaction at the transfer zone often causes

---

Environmental Engineering, Massachusetts Institute of Technology, Cambridge MA 02139-4307 USA; e-mail: sakdiat@mit.edu

detrimental impact forces and excessive dynamic actions (Remennikov and Kaewunruen, 2008; Kaewunruen and Remennikov, 2008; 2009a; 2009b; 2010). Recent studies showed that it is very likely that a railroad turnout bearers or crossties could be subjected to severe impact loads, resulting in a rapid deterioration of its structural integrity and durability (Esveld, 2001; Kaewunruen, 2007; Kaewunruen et al., 2014). Traditional turnout generally imparts high impact forces on to structural members because of its blunt geometry and the gaps between mechanical connections between closure rails and switch rails (i.e. heel-block joints). Although a new method of geometrical design has been adopted for tangential turnouts, the transfer zone at a crossing nose in complex turnout system still imposes high-frequency forces to track components. Generally, the turnout bearers for supporting points and crossing structures were designed using the beam on elastic foundation analysis or 2-D FE grillage modelling (Manalo et al., 2012). Kaewunruen (2014a; 2014b) indicated from recent authority work that some additional factors were often neglected from the grillage analyses, although they must be taken into account, including:

- Extra length of turnout bearers in comparison with standard sleepers
- Centrifugal forces through curved pairs of rails
- Forces and bending moments induced from points motors and other signaling equipment
- Impact forces induced by wheel-rail interaction
- Mechanical rail joints.

This investigation arose from an emerging risk of broken concrete bearers on a mixed-traffics line in New South Wales (NSW), Australia. Due to the complexity of the loadings and damage modes in railway turnouts, this study aims to establish a three dimensional (3D) Finite-element (FE) model. The 3D FE model will adopts an elasto-plastic region of bending and shear deformation of materials. The 3D FE model was developed based upon a common tangential turnout used in Australia. The finding confirms that the crossing panel is where turnout bearers experience the greatest bending moment and shear force (Iwinicki et al., 2009). Despite a large number of investigations, there exists no report on torsional effect on damages of turnout components in the real world (Sae Siew et al., 2015). A highlight of this study is the torsional effect on the turnout structure where improved resiliency will help suppress such an important effect (Kaewunruen, 2012, 2014c; Nimbalkar et al., 2012). The findings will enhance public safety in railway networks with turnouts and crossings.

Finite Element (FE) Modelling

A previous research carried out by Manalo et al. (2010, 2012) analysed the turnout system utilising a grillage beam method. The research was carried out taking in consideration the build and specification of rail used in Queensland, Australia. Results obtained in the study showed that the maximum bending moment and shear force can be witnessed within the switch panel. The results using the grillage beam method seem to have discrepancies with the field observations where the maximum bending and shear forces were evident within the crossing panel (Kaewunruen, 2012). A number of research has been conducted to locate the critical section within a turnout, and many of which conclude upon the critical section being located specifically at the crossing panel (Kassa and Nielsen, 2009; Wiest et al., 2008a; Xiao et al., 2011).

This paper presents the 3D FE analysis using ABAQUS® considering the whole turnout which fully comprises of sleepers, rail, guard rails, crossing nose, rail pads, baseplates and guardrail support plates. The benefits of modelling in 3D are to incorporate the effects of the neighbouring sleepers and to take in consideration the longitudinal forces of the continual rail. The boundary conditions of the central 3D model can be simulated enabling vibrations to radiate beyond the model (Karlsson and Sorensen, 2006).

Wheel/rail interface (W-R)

General track design is based upon the consideration of static axle loads, total sum of axle loads, and running speeds of vehicles as dependant variables. The standard also specifies that vertical static forces are to be designed to accommodate for the combined loading of static wheels, wheel diameters and wheel tread profiles, and for these loading to not jeopardise the safety of the track system by causing excessive stresses and deformation under all normal track conditions. Andersson and Dahlberg (1998) established a linear FE model with modal damping that focuses on the vertical dynamics of a train passing through a turnout. Results showed that the rail discontinuity causes an impact increase between wheel and rail, referred to as a ‘jump’. The condition of the wheel and rail greatly influences the W-R contact force, for the greater the irregularities, the larger the contact force produced. The greater contact force will accelerate the wear and/or crack growth rate in the turnout crossing. Sun et al. (2010) provided an insight on the potential sites for impact and fatigue damage as the train wheel traverses through the nose of the crossing. Firstly, the wing rail fatigue damage is caused by contact from the far side of wheel. Secondly, the transition of the wheel between the wing rail and nose causes a dipping movement. This is due to the tracking on the wing rail to an upward motion on the ramp of the nose resulting in fatigue damage. Greater contact stress can be seen due to the acute contact area in the crossing nose. It is noteworthy that the crossing process will only force the wheel in contact to dip. The British Railways Board (Cherkashin et al., 2009) expressed that the permissible track forces (P_2) for railway vehicles negotiating a discontinuity in rail profile to not exceed 322 kN whilst operating at its maximum design speed. The P_2 force is calculated using the following formula:

$$P_2 = Q + (A_z.V_m.M.C.K) \tag{1}$$

Where

$$M = \left[\frac{M_v}{M_v + M_z}\right]^{0.5} \tag{2}$$

$$M = \left[\frac{M_v}{M_v + M_z}\right]$$

$$C = \left[\frac{\pi.C_z}{4[K_z(M_v + M_z)]^{0.5}}\right] \tag{3}$$

$$K = (K_z.M_v)^{0.5} \tag{4}$$

the lesser of $Q = 0.13D \times 10^3$ or $Q = 125 \times 10^3$ (5)

Where D is the wheel diameter (mm), Q is the maximum static wheel load (N), V_m is the maximum normal operating speed (m/s), M_v is the effective vertical unsprung mass per wheel (kg), A_z is total angle of vertical ramp discontinuity taken as 0.02 rad, M_z taken as 245 kg as the effective vertical rail mass per wheel, C_z taken as 55.4x10^3 N/m as the effective vertical rail damping rate per wheel and K_z taken as 62x10^6 N/m as the effective vertical rail stiffness per wheel.

Lateral forces are designed as to not jeopardise the structural integrity of the rail and track. Unless supported by appropriate technical justification, vehicles attempting to negotiate a lateral ramp discontinuity in track alignment, when travelling on a curve at maximum normal operating speed and at maximum cant deficiency, without exceeding a total lateral force level per axles of 71 kN, and is to be calculated using the following formula:

$$Y = W.A_d + A_y.V_m\left[\frac{M_u}{M_u + M_y}\right]^{0.5}.[K_y.M_u]^{0.5} \tag{6}$$

Where Y is the lateral force per axle (N), W is the static axle load (N), A_d is the maximum normal operating cant deficiency angle (rad), V_m is the maximum normal operating speed (m/s), M_u is the effective lateral unsprung mass per axle (kg), A_y is taken to be 0.0038 rad which is the angle of lateral ramp discontinuity, M_y taken as 170 kg and is the effective lateral rail mass per wheel and K_y taken as 25x10^6 N/m as the effective lateral rail stiffness per wheel.

Turnout Components

The FE model comprises of entirely 3D deformable solids; straight and curved rail, sleepers of varying length and a ballast layer as the track support. This study focuses on the behaviour of the sleeper and ballast; therefore, a suitably accurate rail seat load within a tangential configuration is required for the analysis. Steel rails were modelled in 3D to account for its cross sectional properties, the width of the contact patch between the wheel and rail, the width of the rail web and the width of the rail footing. The rail and switch rail profiles were validated against rail authority's specifications (RailCorp, 2012a, 2012b, 2012c). Concrete bearers have been modelled as rectangular blocks with dimensions nominated according to the specifications varying lengths between 2.5 m to 7.5 m according to the turnout design as tabulated in Table 1.

The elastic modulus of steel rails and crossing is defined by the initial slope of the stress-strain relationship to the extent of the upper yield threshold, as illustrated in Figure 2. For concrete material, it is assumed that its compressive stress behaviour is to be linear given that is does not exceed $0.4f'_c$. Beyond the linear threshold, stress is expressed as a function of strain accordingly to Equation (7). A graphical representation of the stress-strain relationship of concrete is depicted in Figure 3.

$$\sigma_c = \frac{f'_c \gamma (^{\varepsilon_c}/_{\varepsilon'_c})}{\gamma - 1 + (^{\varepsilon_c}/_{\varepsilon'_c})^{\gamma}} \tag{7}$$

where $$\gamma = \left|\frac{f'_c}{32.4}\right|^3 + 1.55 \text{ and } \varepsilon'_c = 0.002 \tag{8}$$

Indraratna and Nimbalkar (2011) proposed an idealisation of the ballast layer as a hardening-soil (HS) model. This method is an advanced method in analysing the mechanical behaviour in soil as it considers the plasticity theory, along with the effect of viscosity on the shear strain and a yield cap. Because this analysis focuses mostly on an elastic range, the evaluation takes upon the approach of simplifying the ballasted track support using elastic solid elements. A track support modulus of 50 MPa is adopted to comply with the design requirements and field data (RailCorp, 2012a, 2012b).

Boundary Conditions

A sensitivity analyses has been undertaken for mesh sizes for each rail components. As the mesh sizes and the material densities are different between the two tied objects, a tie constraint is generated to allow for ABAQUS® to automatically optimise and refine the interface mesh. Tie constraints are applied to the rail and the concrete sleepers to represent the rail fastener. Instead of frictional interaction and the effect of submersed sleepers in a ballast layer, the sleepers are tied onto the underlying ballast layer to greatly reduce computational effort. As all members are tied, translational and rotational degrees of freedom will be equal throughout. All tie constraints will be taken to be surface to surface, as opposed to a simplified node to surface, as this will allow for uniform distribution between the tied components (Karlsson and Sorensen, 2006).

A fixed boundary condition is applied to the bottom most surface of the ballast to idealise the substructure and a symmetrical constraint is applied to the ends of the rail to idealise a continuous rail within the relevant plane, in this case the Z-axis. The sleepers are attached to other members with boundary constraints, and they can deform freely with the ballast bed.

Load Conditions

The FE model predicts the behaviour of the turnout by considering multi-wheel impacts which would simulate in-service and cyclic loading, and will be adapted as a set of concentrated loads negotiating the turnout to represent a moving coupled locomotive. Loading configuration is in accordance with Standards Australia (2004), using the contact position to generate the maximum impact force. Design loads can be depicted in Figure 4a, which simulate the worst case loading configuration that can be exerted onto a rail track. The coupled locomotive is simulated with four 300 kN axle loads and a single 360 kN axle load 2 meters ahead of the group.

The above load set is applied to the model at 600mm increments, or referred hereafter as load sets. A total of 48 load steps (including model initiation) have been modelled to generate the overall movement of the locomotive negotiating the turnout. Figure 4b illustrates loading configurations for particular steps.

Validation

The deflection of the sleeper is dependent on the mesh sizes of the ballast; the ballast serves as a slave surface in which the sleeper is modelled to suppress into. Along with an accurate resultant deflection, the time required to compute the analysis is also significant in selecting an optimum mesh size. It is noted that the typical aggregate size of ballast is anywhere between 13 mm to 65 mm (RailCorp, 2012a). An initial analysis was carried out to determine the maximum deflection under the said design train loading. A mesh size of 80 mm x 80 mm had been nominated. Figure 5 below shows the maximum vertical deflection, taken at the mid-point of each sleeper, with a single pass of the coupled locomotive load. The results show that sleeper number 47 (out of a total of 51 sleepers), which is located directly underneath the crossing nose, is subjected to the greatest deflection. The next step in analysing the sleeper behaviour would be to assess the deflection in relations to the location of the load, in this case as a function of load step. The deflection response is presented graphically in Figure 6. It can be seen that the sleeper does not undergo any translations up until the 35^{th} load step. This is an important step in dramatically reducing the computational time required to analyse the model with different mesh sizes. As we had located the critical sleeper in the preliminary test, it is advantageous to exclude all previous steps between the initial and 34^{th} step from the analysis in determining optimum mesh size as this will reduce the computational time by almost 80%. Table 2 lists the maximum deflection of the chosen sleeper under train loading according to varied mesh sizes and Figure 7 depicts the critical response between load steps 35 to 47.

It can be seen from the results above that the change in the mesh size does not significantly affect the maximum deflection as seen by the largest deviation (< 0.3 mm) that is negligible. As previously mentioned, computational time is taken into great consideration, and it can be seen that although the 60 mm and 100 mm mesh yield the same result, the former takes almost 4.5 times the amount of time to compute compared to the latter. Given this, the 100 mm x 100 mm mesh will be accurate and the most efficient for this study purpose. Note that the track stiffness of this model has been benchmarked with the field measurement (Sae Siew et al., 2015).

Results and Discussion

Field observations suggested that impacts at turnout crossing frequently cause the most maintenance of supporting bearers and fastening systems. These impacts are due to the wheel rail interaction over the transfer zone (Kaewunruen, 2014a, 2014b). The FE model, which has been developed to simulate a turnout system subjected to a moving design load, reveals similar results. It is found that the sleepers, which undergo the greatest deflection of a coupled locomotive pass, are the sleepers underneath the crossing nose (maximum at sleeper #47). The sensitivity analysis illustrates the maximum deflection in all sleepers with the passing of a moving couple train load, 300LA (Standards Australia, 2004). From this analysis, it can be seen from Figure 8 that sleeper 47 experiences the greatest deflection, with a resultant of 2.54 mm. Figure 9 illustrates the deflection response of the critical sleeper (47) in terms of the location of train, or load step. The sharp spike in deflection clearly defines the moment at which each wheel axle impacts the above rail, in this case the crossing nose.

The direction of translations is also an important factor, especially when predicting the long-term stability of the ballast layer. It can be seen from the deflection shapes depicted in Figures 10 and 11 that the translation are not vertical, and tend to suggest the whole movement of the sleeper to be a rotation or a twist.

Figure 12 further explores the effects of the sleeper deflection into the underlying ballast layer. The below deflection is a resultant of 300LA loading (Standards Australia, 2004) as the front axle impacts the crossing nose, to then exit the turnout on the diverging track. The stress parameters are calculated based on the Von Mises yield criterion, which was explained in earlier section. Examples of the shear stress distribution for a particular load step along the turnout system are detailed below in Figure 13. Shear stress within this particular model is about the XY plane, *S12, or*σ_{12}. The resultant stresses are based upon critical loading configuration. It is found that the sleeper, which experiences the greatest shear and bending moment, is found to be the one directly underneath the crossing nose (sleeper 47). It is important to note that torsional behaviour observed is likely caused by the crossing angle, which influences wheel/rail contact path and the loading location.

The critical sleepers within the specified length have been chosen accordingly to the maximum resultant deflection during one passing of a moving load. The largest deflection in a sleeper of lengths 2.6-2.8 metres has been recorded within sleeper 21 (sleeper right underneath the heel joint), resulting in a maximum deflection of 1.28 mm. The largest deflection recorded within the range of 2.801-5.200 metres has been established earlier as the critical sleeper, sleeper 47. The maximum deflection values are generated using the sleeper deflection with relation to the load steps. Critical loading occurs during load step 36 for sleeper 47 (sleeper right underneath the crossing during the passage of a running wheel), and load step 18 for sleeper 21 (sleeper right underneath the heel joint during the rapid change of train direction).

Conclusions

This paper presents a part of the investigation that is arisen from the field observations and measurements on a mixed traffic rail line where broken concrete bearers and loosen fasteners were reported routinely. A 3D FE model has been established for the analysis of a complete turnout system. The primary objective of this study was to determine the critical location; be able to realise the critical deflection, and validate shear force and bending moment envelopes of a turnout system. To address this, ABAQUS® was employed to carry out all modelling and post-processing of a complete 3D turnout.

Through the sensitivity analysis, it is clear that turnout bearers right underneath crossing panel experience the highest load actions, resulting in the largest deformations. Importantly, we are the first to report that the cute angle of crossing nose also induces torsional force on the supporting track structure. Although the torsion can be coped with by the ballast aggregates, such an effect causes damages to fastening systems and the bearers as evidenced in practice. Future work will evaluate the effects of dimension, topology and stiffness of fastening systems to mitigate the torsional crossing impacts.

Acknowledgement

The authors are grateful to University of Western Sydney and RailCorp for the support throughout this study. Also, the third author wishes to thank Australian Government for his Endeavour Executive Fellowships at Massachusetts Institute of Technology, Harvard University, and Chalmers University of Technology.

References

Andersson, C. and Dahlberg, T. 1998. Wheel/rail impacts at a railway turnout crossing. *Proceedings of the Institution of Mechanical Engineers,* 212**,** 123-134.

Cherkashin, U., Zakharov, S. & Semechkin, A. 2009. An overview of rolling stock and track monitoring systems and guidelines to provide safety of heavy and long train operation in the Russian Railways. *Proceedings of the Institution of Mechanical Engineers, Part F: Journal of Rail and Rapid Transit,* 223**,** 199-208.

Esveld, C., 2001. *Modern Railway Track,* The Netherlands MRT Press.

Indraratna, B. & Nimbalkar, S. 2011. Implications of ballast breakage on ballasted railway track based on numerical modelling.

Iwnicki, S., Bezin, Y., Xie, G. & Kassa, E. 2009. Advances in vehicle-track interaction tools. *Railway Gazette International,* 165**,** 47-49,51-52.

Kaewunruen, S. 2007. Experimental and numerical studies for evaluating dynamic behaviour of prestressed concrete sleepers subject to severe impact loading. *PhD Thesis*, School of Civil, Mining, and Environmental Engineering, University of Wollongong, Australia.

Kaewunruen, S. 2012. Effectiveness of using elastomeric pads to mitigate impact vibration at an urban turnout crossing, in Maeda et al. (Eds.) Noise and Vibration Mitigation for Rail Transportation Systems, Springer, 357-365.

Kaewunruen, S. 2014a, "Monitoring structural deterioration of railway turnout systems via dynamic wheel/rail interaction." Case Studies in Non-destructive Testing and Evaluation, in press.

Kaewunruen, S. 2014b, "Monitoring in-service performance of fibre-reinforced foamed urethane material as timber-replacement sleepers/bearers in railway urban turnout systems." Structural Monitoring & Maintenance, 1(1): 131-157 (invited).

Kaewunruen, S. 2014c, "Discussion of ‘Mitigation of Ground Vibration Generated by High-Speed Trains on Saturated Poroelastic Ground with Under-Sleeper Pads’." ASCE Journal of Transportation Engineering, in press.

Kaewunruen, S. & Remennikov, A. M. 2006. Sensitivity analysis of free vibration characteristics of an in situ railway concrete sleeper to variations of rail pad parameters. *Journal of Sound and Vibration,* 298**,** 453-461.

Kaewunruen, S. & Remennikov, A. M. 2007. Investigation of free vibrations of voided concrete sleepers in railway track system. *Proceedings of the Institution of Mechanical Engineers,* 221**,** 495-507.

Kaewunruen, S. and Remennikov, A.M., 2008, Nonlinear transient analysis of railway concrete sleepers in track systems. *International Journal of Structural Stability and Dynamics*, 8(3): 505-520.

Kaewunruen, S. and Remennikov, A.M., 2009a, "Progressive impact behaviours of prestressed concrete sleepers in railway track environments." Engineering Structures, 31(10):2460-2473.

Kaewunruen, S. and Remennikov, A.M., 2009b, "Impact fatigue responses of pre-stressed concrete sleepers in railway track systems." The IES Journal Part A: Civil & Structural Engineering, 2 (1), 47-58.

Kaewunruen, S. and Remennikov, A.M., 2010, "Dynamic crack propagations of prestressed concrete sleepers in railway track systems subjected to severe impact loads." ASCE Journal of Structural Engineering, 136(6): 749-754.

Kaewunruen, S. and Remennikov, A.M., 2013, "On the residual energy toughness of prestressed concrete sleepers in railway track structures subjected to repeated impact loads." Electronic Journal of Structural Engineering, 13(1): 31-47.

Kaewunruen, S., Remennikov, A.M., Aikawa, A., and Sakai, H., 2014, "Free vibrations of interspersed railway track systems in three-dimensional space." Acoustics Australia, 42(1): 20-26.

Karlsson and Sorensen 2006. *ABAQUS/CAE User's Manual: Element*, Pawtucket, Rhode Island, Hibbitt Publication.

Kassa, E. & Nielsen, J. 2008a. Dynamic interaction between train and railway turnout: full-scale field test and validation of simulation models. *Vehicle System Dynamics,* 46**,** 521-534.

Kassa, E. & Nielsen, J. C. O. 2008b. Stochastic analysis of dynamic interaction between train and railway turnout. *Vehicle System Dynamics,* 46**,** 429-449.

Kassa, E. & Nielsen, J. C. O. 2009. Dynamic train–turnout interaction in an extended frequency range using a detailed model of track dynamics. *Journal of Sound and Vibration,* 320**,** 893-914.

Manalo, A., Aravinthan, T., Karunasena, W. & Stevens, N. 2012. Analysis of a typical railway turnout sleeper system using grillage beam analogy. *Finite Elements in Analysis & Design,* 48**,** 1376.

Nimbalkar, S., Indraratna, B., Dash, S. & Christie, D. 2012. Improved Performance of Railway Ballast under Impact Loads Using Shock Mats. *Journal of Geotechnical and Geoenvironmental Engineering,* 138**,** 281-294.

Railcorp Nsw 2012a. ESC 240. *Ballast.* Rail Corporation of New South Wales.

Railcorp Nsw 2012b. ESC 250. *Turnouts and special trackwork.* Rail Corporation of New South Wales.

Railcorp Nsw 2012c. SPC 233. *Concrete turnout bearers.* Rail Corporation of New South Wales.

Remennikov, A. M. & Kaewunruen, S. 2008. A review of loading conditions for railway track structures due to train and track vertical interaction. *Structural Control and Health Monitoring,* 15(2)**,** 207-234.

Sae Siew, J., Mirza, O., Kaewunruen, S. 2015. Nonlinear finite element modelling of railway turnout system considering bearer/sleeper-ballast interaction. Journal of Structures, ID 598562, http://dx.doi.org/10.1155/2015/598562

Standards Australia 2002. AS 1085.1. *Railway track material - Steel rails.* Standards Australia.

Standards Australia 2004. AS 5100.2. *Bridge design - Design loads.* Standards Australia.

Sun, Y. Q., Cole, C. & Mcclanachan, M. 2010. The calculation of wheel impact force due to the interaction between vehicle and a turnout. *Proceedings of the Institution of Mechanical Engineers,* 224**,** 391-403.

Wiest, M., Daves, W., Fischer, F. D. & Ossberger, H. 2008a. Deformation and damage of a crossing nose due to wheel passages. *Wear,* 265**,** 1431-1438.

Wiest, M., Kassa, E., Daves, W., Nielsen, J. C. O. & Ossberger, H. 2008b. Assessment of methods for calculating contact pressure in wheel-rail/switch contact. *Wear,* 265**,** 1439-1445.

Xiao, J., Zhang, F. & Qian, L. 2011. Numerical simulation of stress and deformation in a railway crossing. *Engineering Failure Analysis,* 18**,** 2296-2304.

List of Figures

Figure 1. Typical components of a railway turnout (after Kaewunruen, 2014a).

Figure 2. Stress-strain relationship of structural steel

Figure 3. Stress-strain relationship of concrete

Figure 4. Railway Traffic Loads - Axle Loads

Figure 5. Mid-point deflections of each sleeper along the turnout

Figure 6. Displacement envelope of the sleeper right underneath the crossing (#47)

Figure 7. Effect of mesh sizes on the deflection of the sleeper right underneath the crossing (#47)

Figure 8. Maximum deflection of sleepers 1-51 under applied moving load

Figure 9. Deflection of critical sleeper (47) in relation to location of load

Figure 10. Deflection mode of critical sleeper - XY plane

Figure 11. Deflection mode of critical sleeper – 3D plane centre cut view

Figure 12. Deflections of ballast layer

Figure 13. Shear stresses of turnout sleepers

Table 1. Design properties of materials

Materials	Elastic modulus (MPa)	Compressive strength (MPa)	Tensile strength (MPa)
Concrete	38,000	36 - 55	4.0 - 6.30
Prestressing tendon	200,000	-	1,700
Steel rails	205,000	-	-

Table 2 Resultant deflection of sleeper 47 and computational time with varying ballast mesh size

Mesh size (mm)	Deflection (mm)	Computational time (s)
60 x 60	2.54	24,784
70 x 70	2.32	12,638
80 x 80	2.28	10,824
90 x 90	2.59	5,655
100 x 100	2.54	5,547

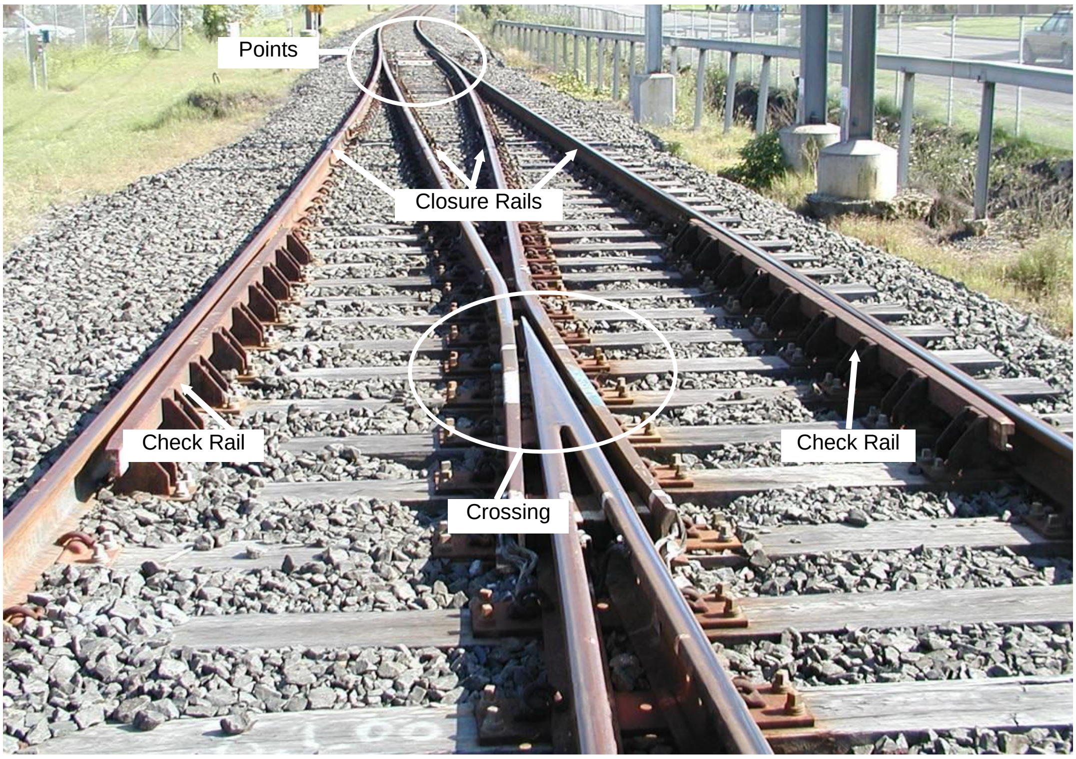

Figure 1. Typical components of a railway turnout (after Kaewunruen, 2014a).

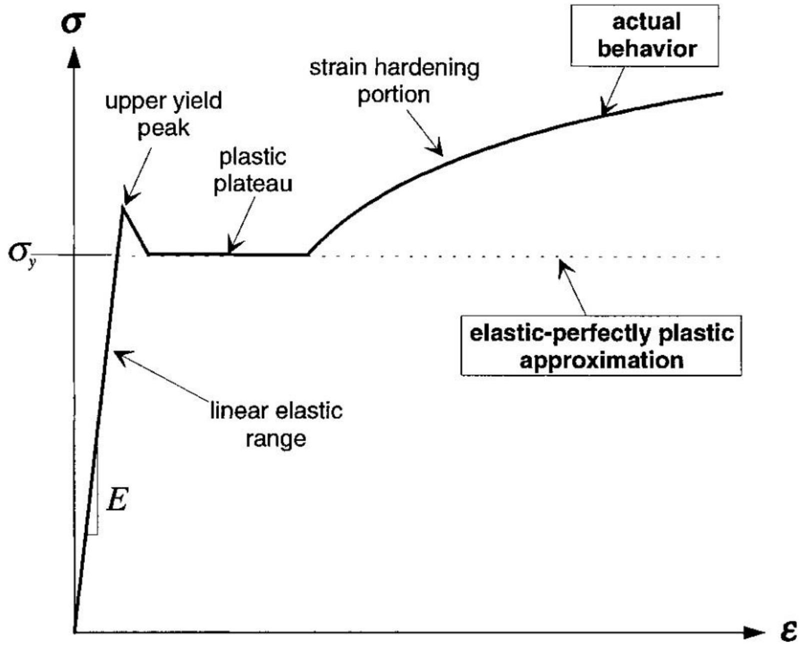

Figure 2. Stress-strain relationship of structural steel

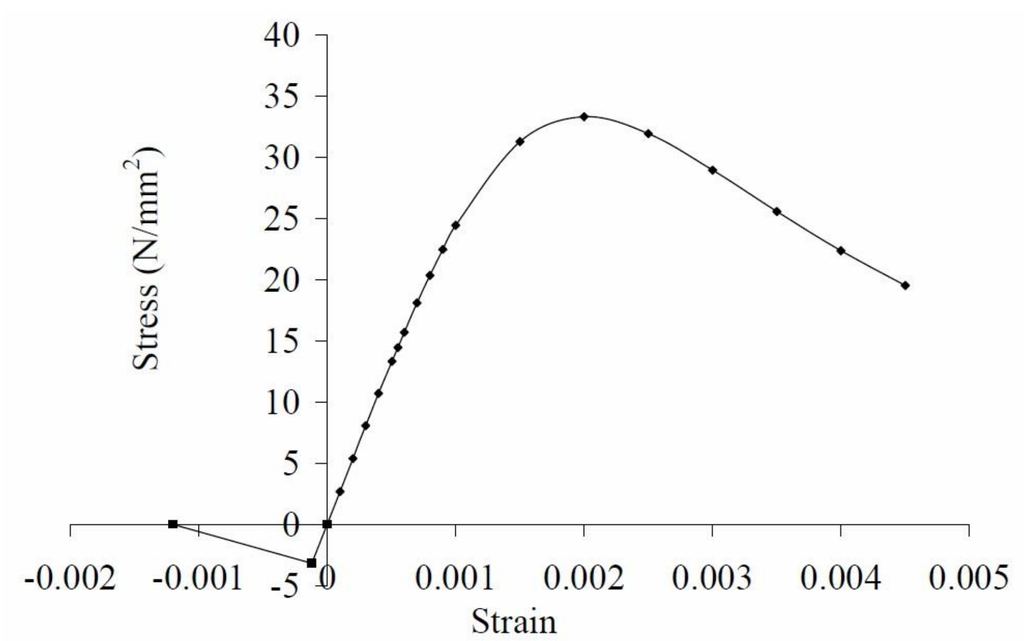

Figure 3. Stress-strain relationship of concrete

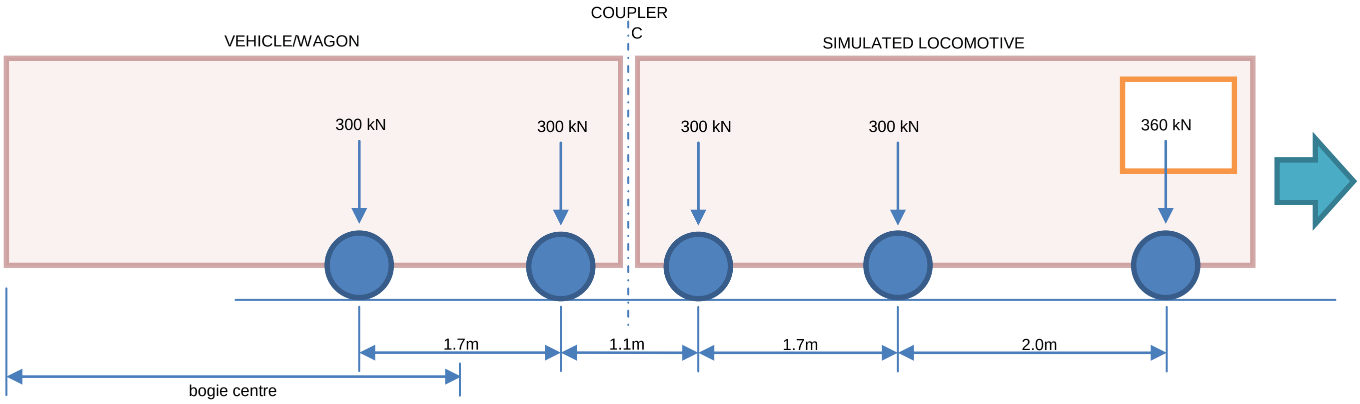

a) 300LA Load case

Figure 4. Railway Traffic Loads - Axle Loads

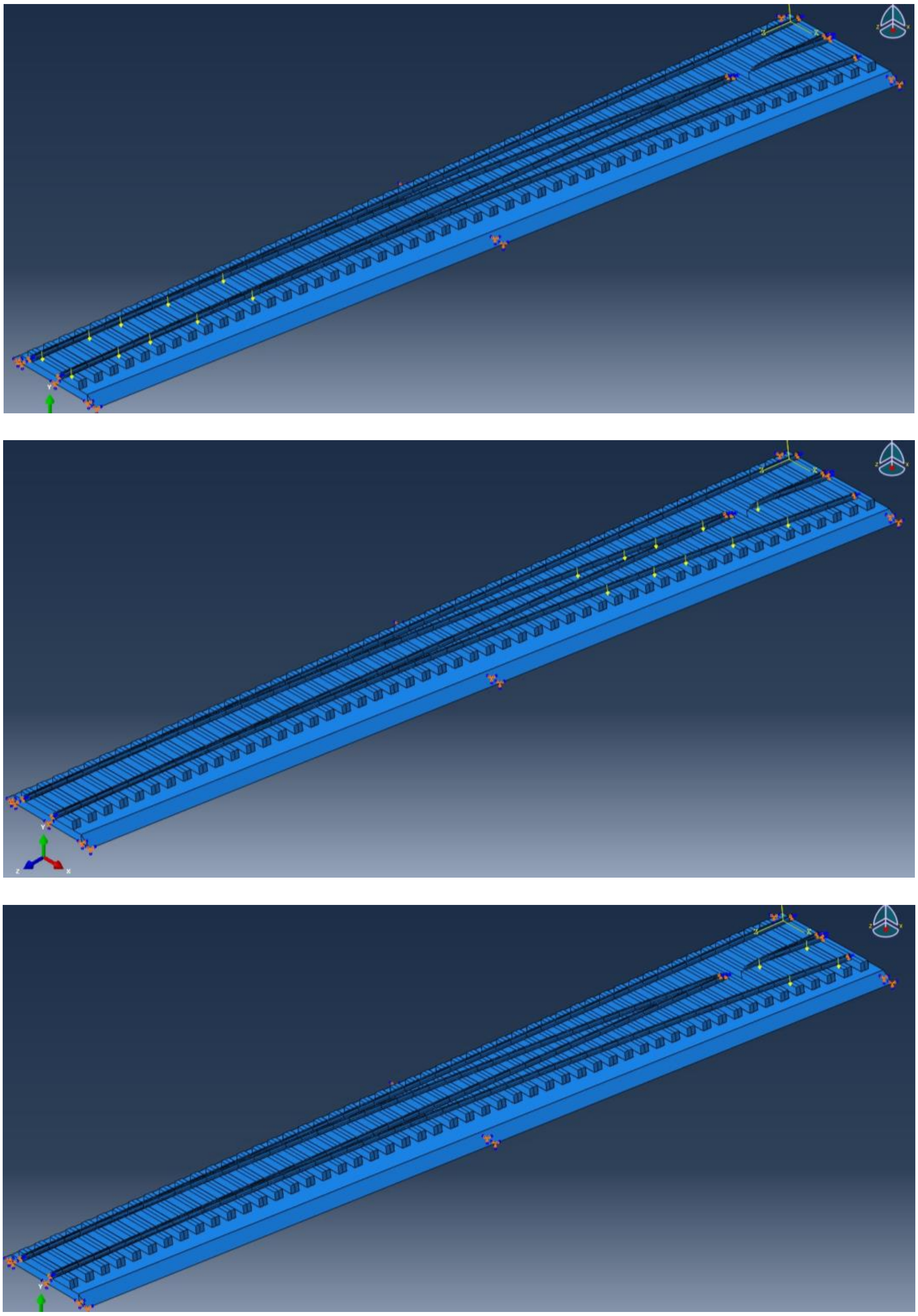

b) Load steps: 300LA coupled locomotive design loading on turnout; (top) load step 2, (middle) load step 36 and (bottom) load step 48

Figure 4. Railway Traffic Loads - Axle Loads

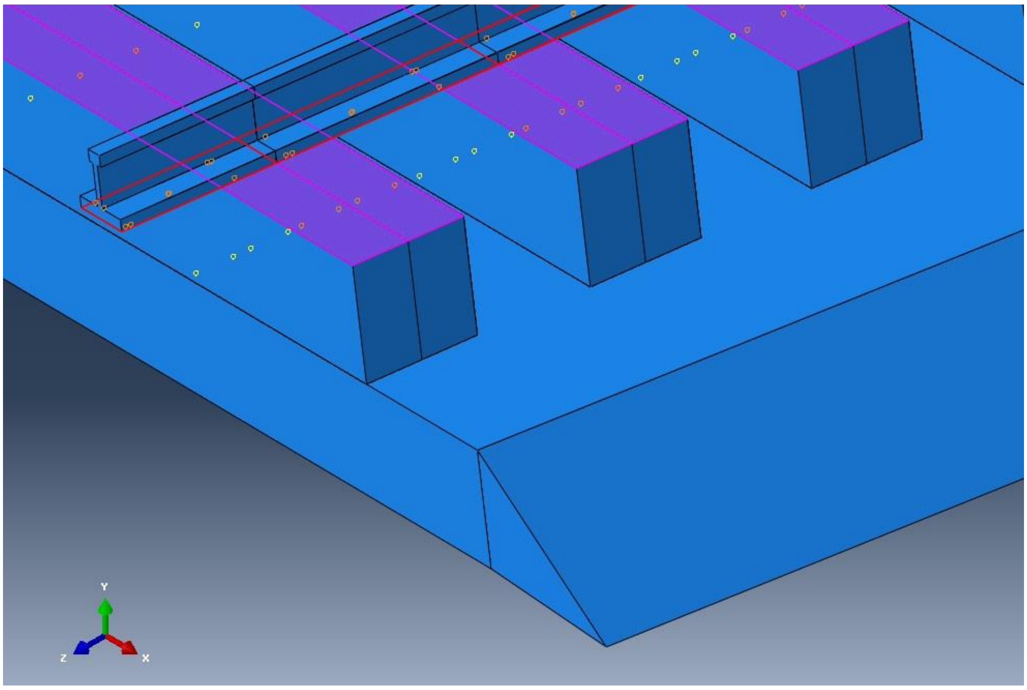

a) Tie constraint between rail and sleeper

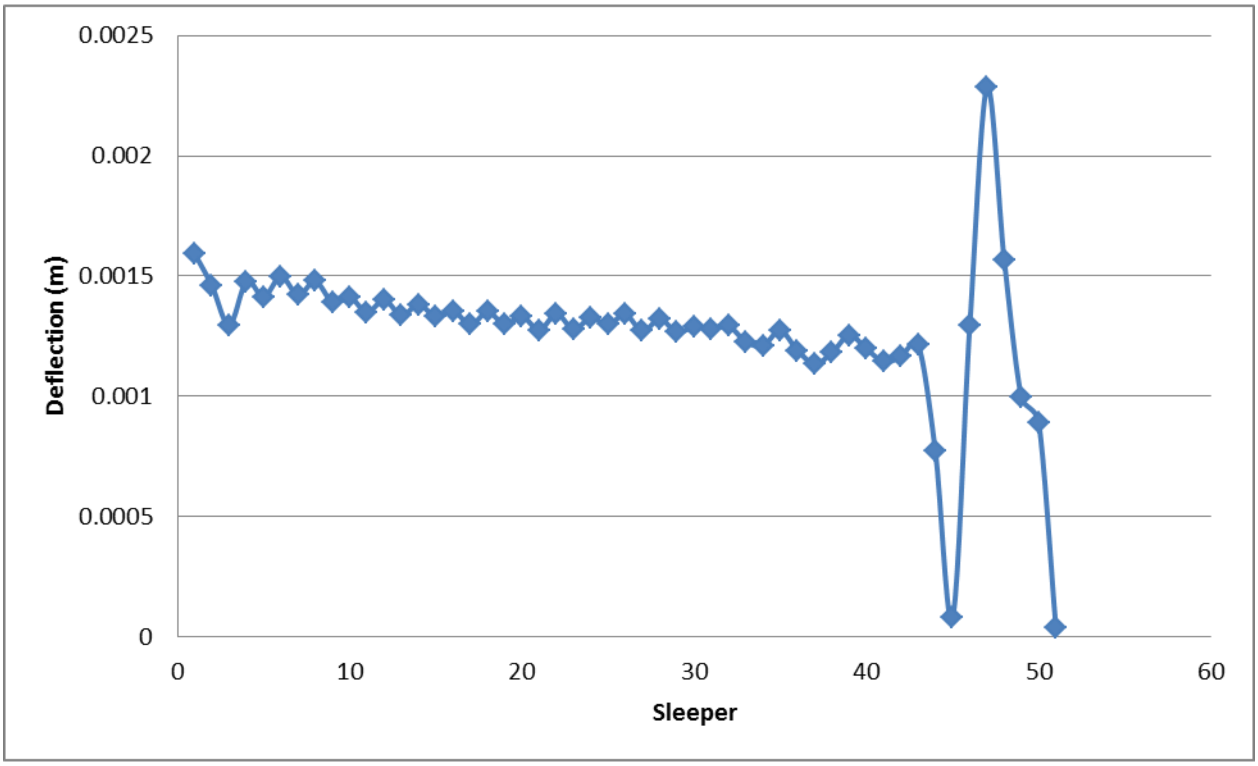

b) Maximum recorded deflection at each sleeper (mid-point)

Figure 5. Mid-point deflections of each sleeper along the turnout

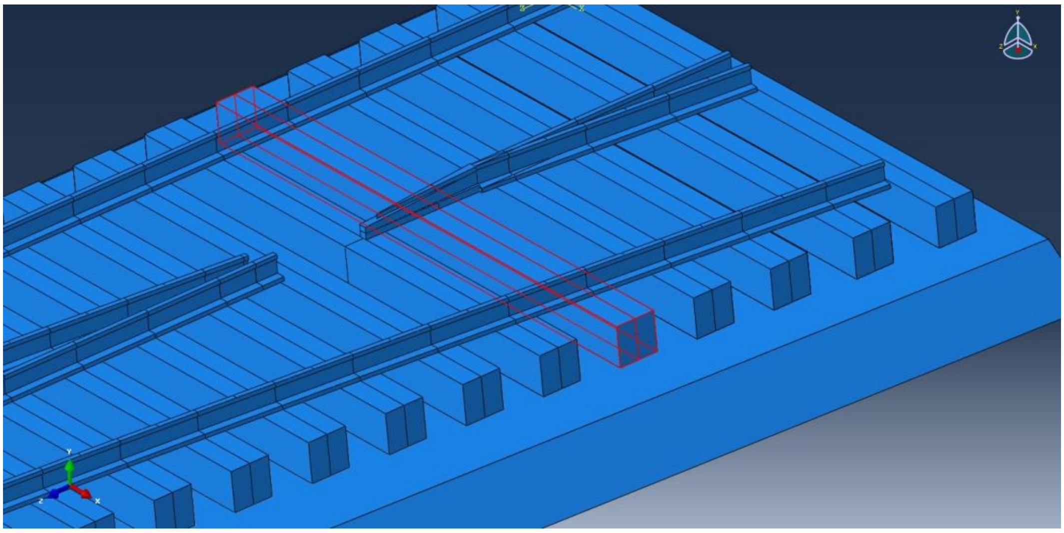

a) Sleeper 47 (red) experiences the greatest deflection

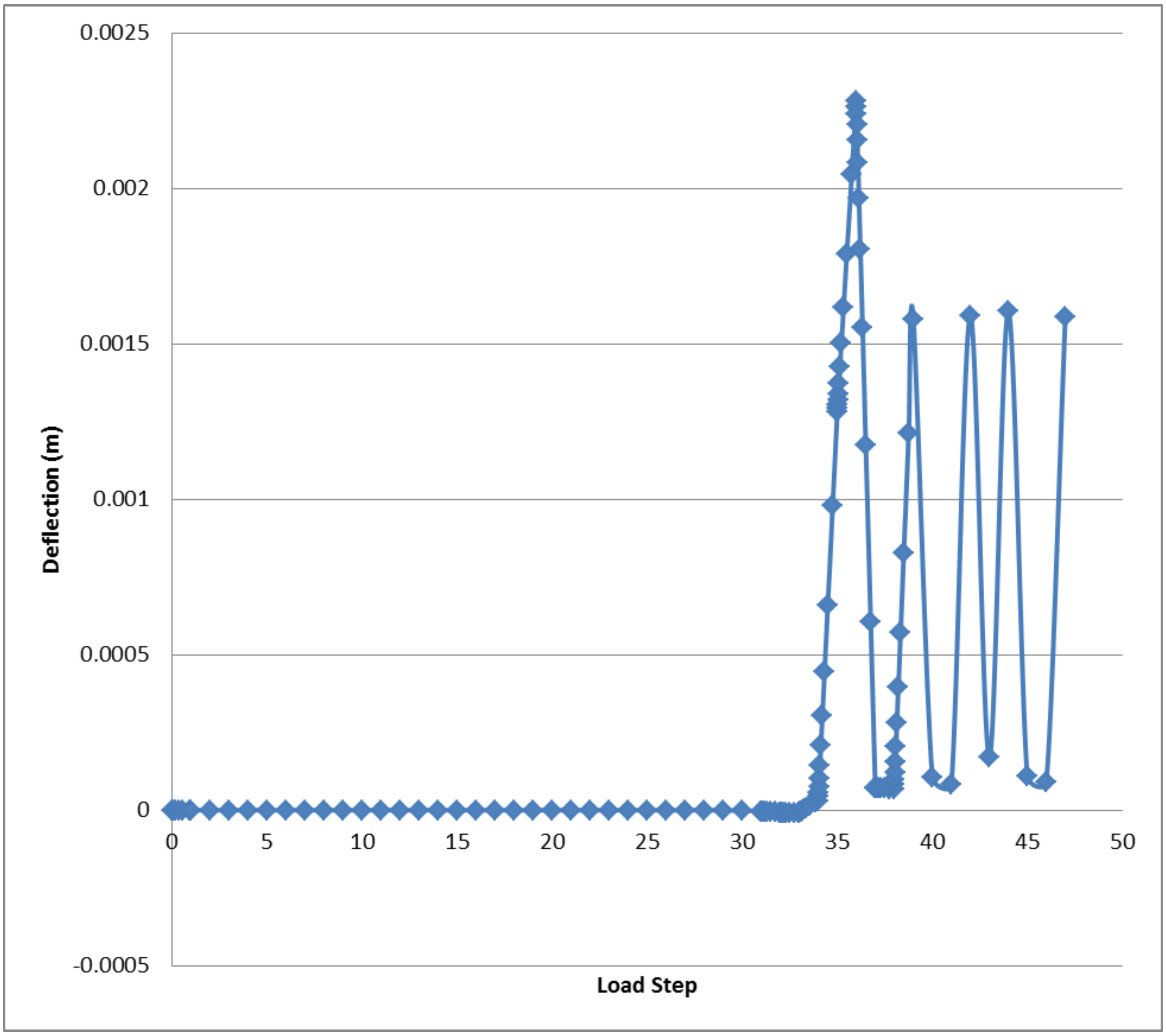

b) Deflection response of Sleeper 47 at each load step

Figure 6. Displacement envelope of the sleeper right underneath the crossing (#47)

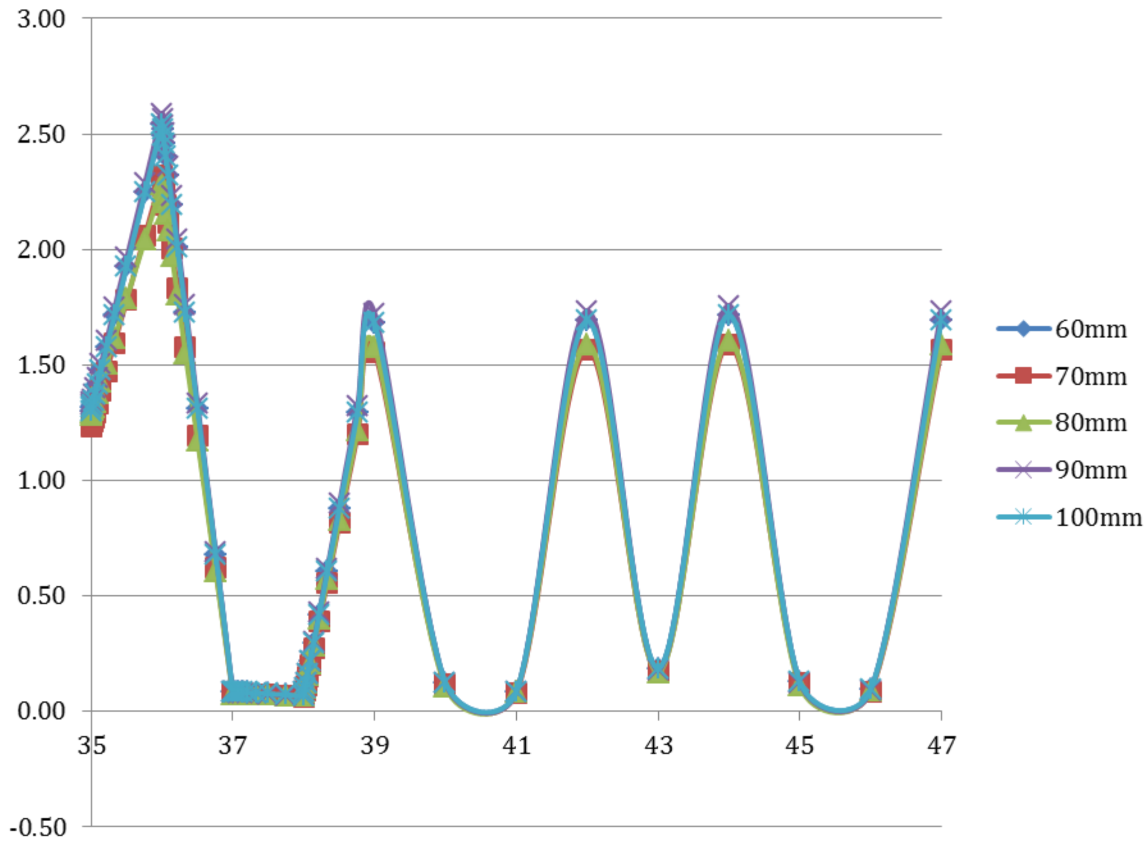

Figure 7 Effect of mesh sizes on the deflection of the sleeper right underneath the crossing (#47)

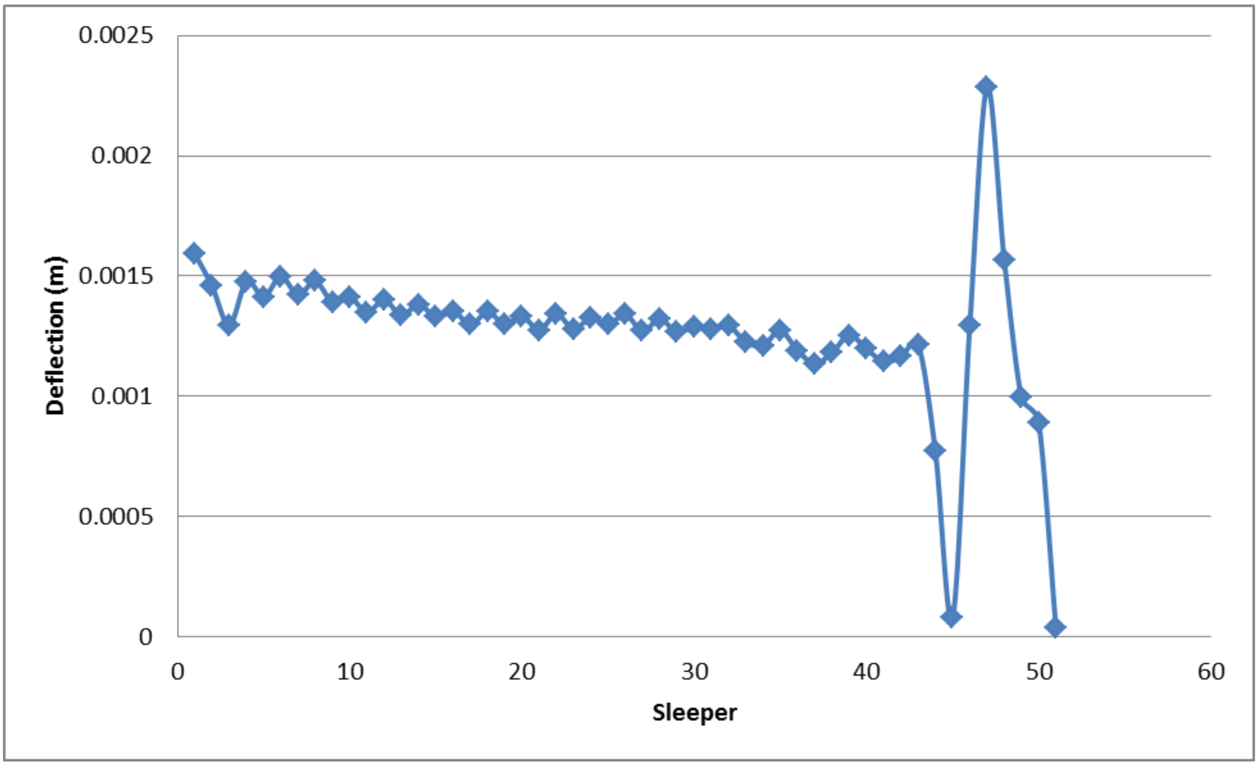

Figure 8 Maximum deflection of sleepers 1-51 under applied moving load

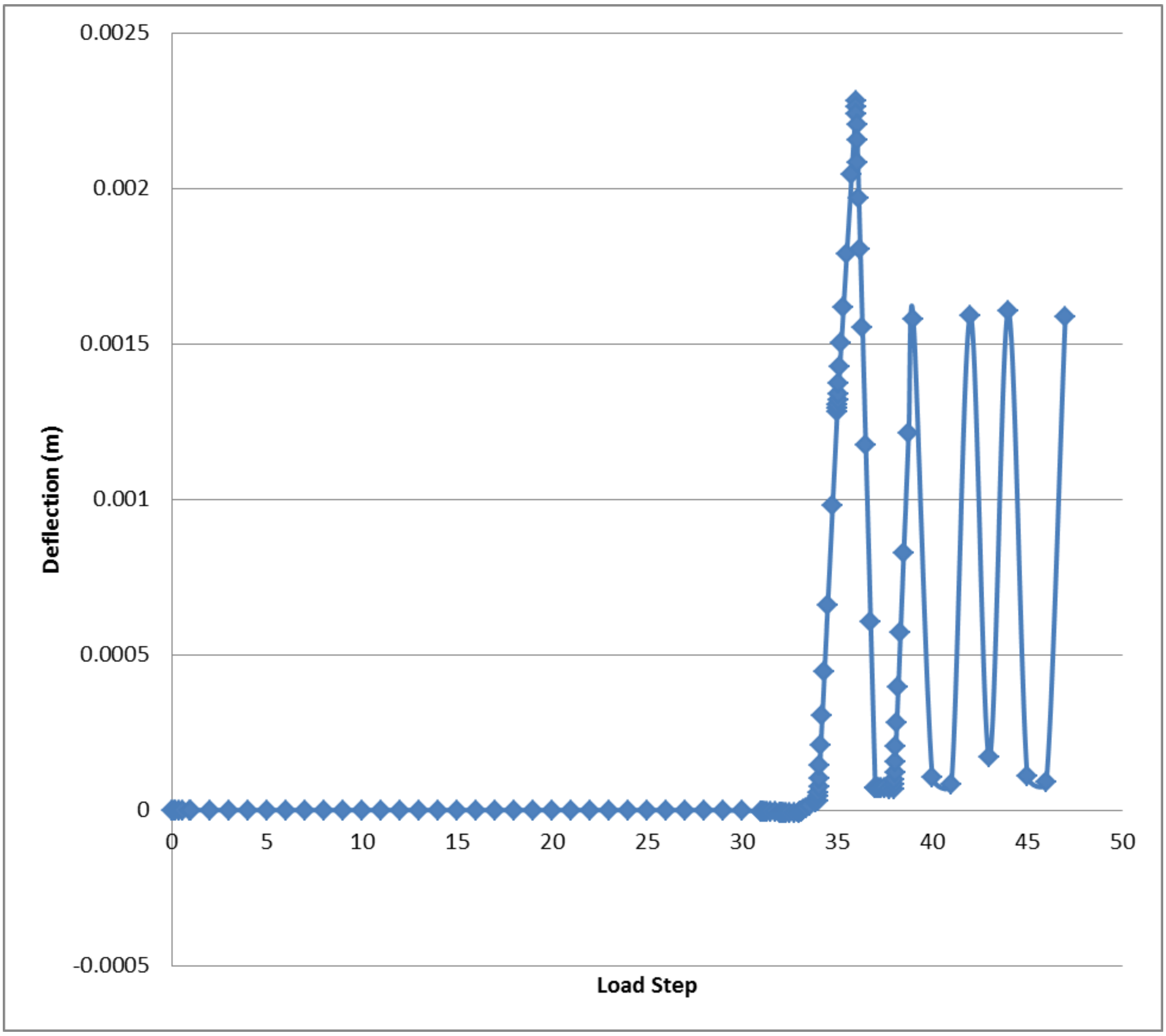

Figure 9 Deflection of critical sleeper (47) in relation to location of load

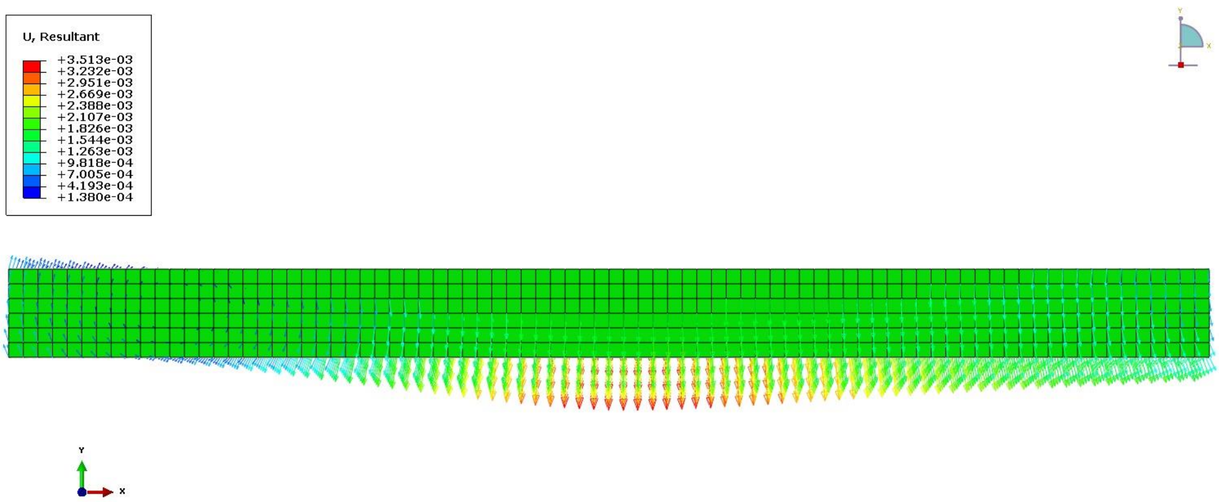

Figure 10 Deflection mode of critical sleeper - XY plane

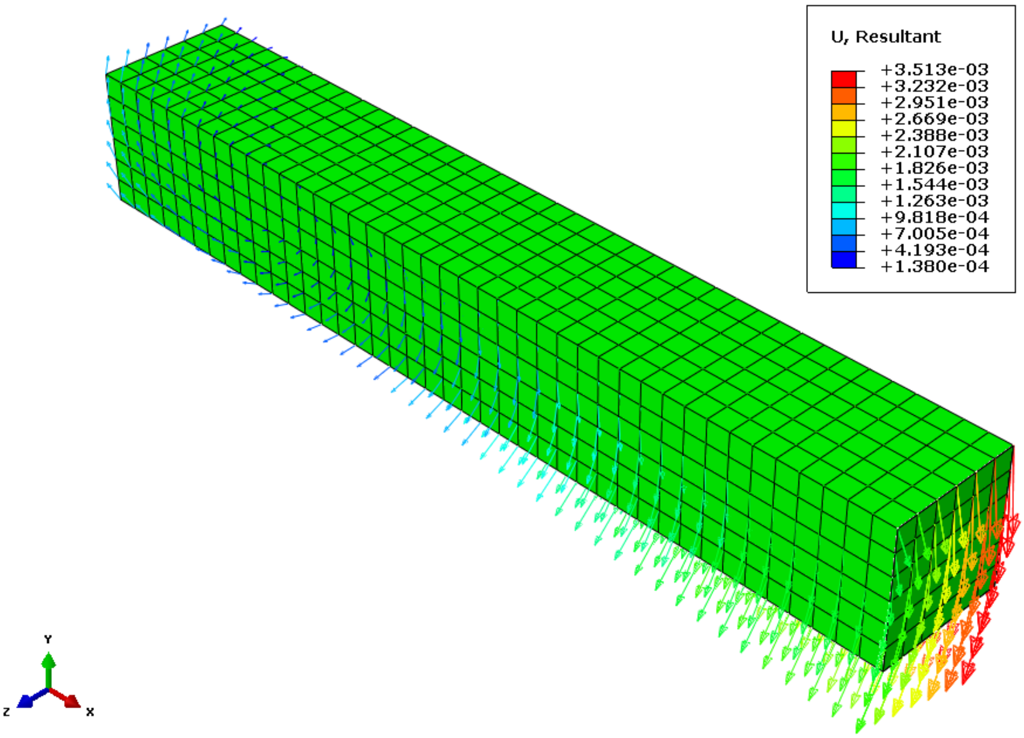

Figure 11 Deflection mode of critical sleeper – 3D plane centre cut view

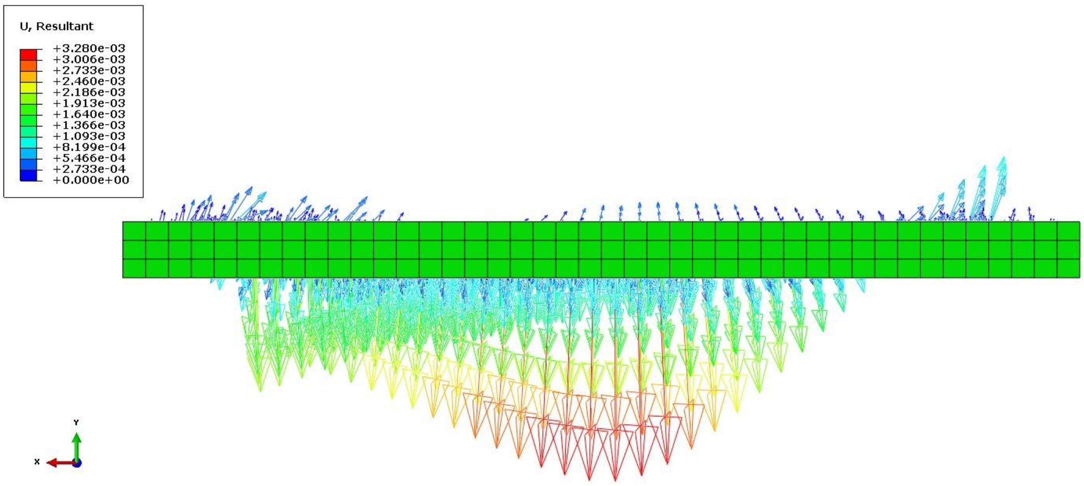

a) Deflection of ballast layer for critical loading - XY plane

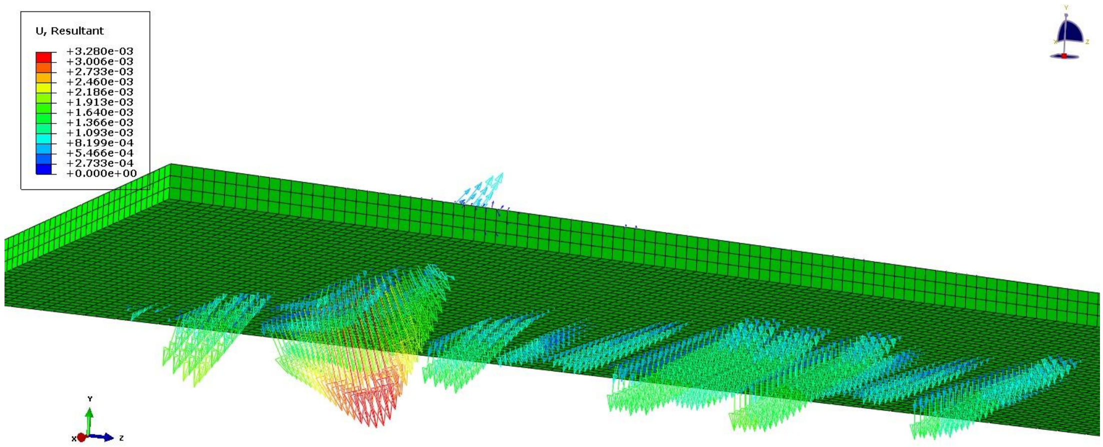

b) Deflection of ballast layer for critical loading - 3D plane

Figure 12 Deflections of ballast layer

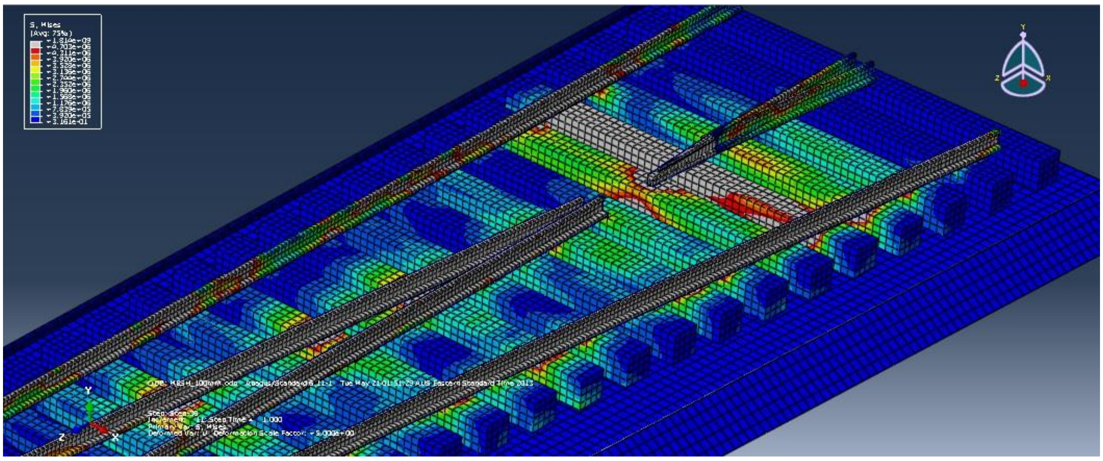

a) Stress distribution at load step 36 for 100mm meshed ballast (when the wheel runs over the crossing nose)

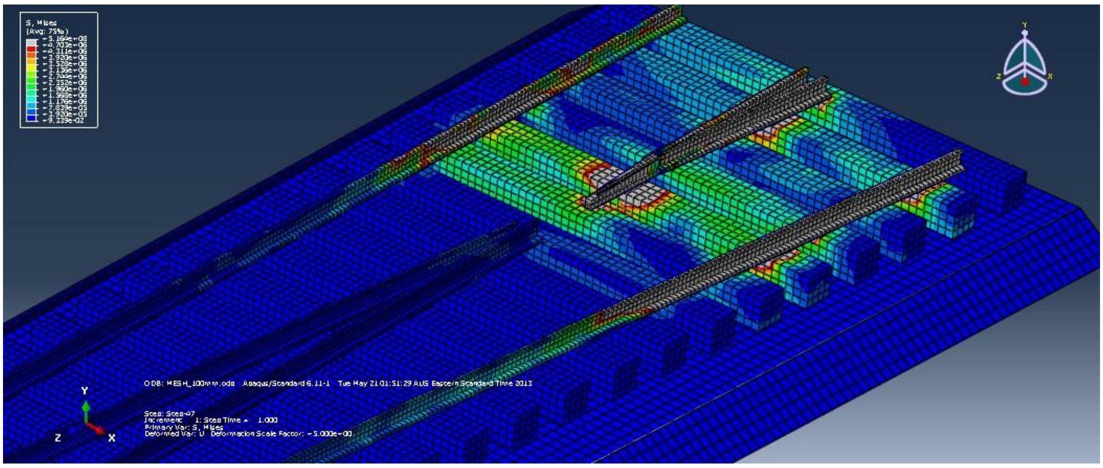

b) Stress distribution at load step 47 for 100mm meshed ballast (when the wheel runs further away from the crossing nose)

Figure 13 Shear stresses of turnout sleepers